

Erik Wächtler, Robert Gericke, Theresa Block, Birgit Gerke, Rainer Pöttgen and Jörg Wagler\*

# Compounds of the types $Pn(pyS)_3$ ( $Pn = P, As, Bi$ ; $pyS$ : pyridine-2-thiolate) and $Sb(pyS)_xPh_{3-x}$ ( $x = 3-1$ ); molecular structures and electronic situations of the $Pn$ atoms

<https://doi.org/10.1515/znb-2020-0171>

Received October 14, 2020; accepted December 12, 2020;

published online January 15, 2021

**Abstract:** The compounds  $Pn(pyS)_3$  ( $Pn = P, As, Sb, Bi$ ) were synthesized from the respective chloride ( $Pn = P, As, Sb$ ) or nitrate ( $Bi$ ), pyridine-2-thiol ( $pySH$ ) and triethylamine ( $NEt_3$ ) as a supporting base in THF ( $P, Sb$ ),  $CHCl_3$  ( $As$ ) or methanol ( $Bi$ ).  $Sb(pyS)_3$  was also obtained from the reaction of  $SbCl_3$  with  $LipyS$  (prepared *in situ*) in methanol. The compounds  $Sb(pyS)_2Ph$  and  $Sb(pyS)Ph_2$  were prepared in a one-pot reaction starting from  $SbCl_3$  and  $SbPh_3$  (1:1 ratio). Upon  $Cl/pyS$  substitution, the resulting reaction mixture allows for a facile separation of the products in hot hexane.  $P(pyS)_3$  and  $As(pyS)_3$  crystallize isostructurally to the reported structure of  $Sb(pyS)_3$  with  $\kappa$ -S-bound  $pyS$  ligands. These crystal structures feature close  $Pn \cdots Pn$  contacts which are most pronounced for the arsenic derivative.  $Bi(pyS)_3$  adopts a different molecular structure in the solid state, which features two chelating ( $\kappa^2$ -S,N- $pyS$ ) ligands and a  $\kappa$ -S-bound ligand. The presence of  $N \rightarrow Bi$  interactions between the nitrogen atom of the  $\kappa$ -S- $pyS$  ligand and the  $Bi$  atom of another molecule renders this structure a polymer chain along the crystallographic  $b$  axis with  $Bi \cdots Bi$  van-der-Waals contacts. The structures of this set of  $Pn(pyS)_3$  compounds were also studied in solution using  $^1H$  NMR spectroscopy, revealing equivalent  $pyS$  ligands in discrete  $Pn(pyS)_3$  molecules. The molecular structure of  $Sb(pyS)Ph_2$

was optimized by quantum chemical methods, and a comparison with the structures reported for the other  $Sb/pyS/Ph$  combinations reveals  $Sb(pyS)_2Ph$  to feature the strongest  $Sb \cdots N$  interactions with the  $\kappa$ -S- $pyS$  ligand. The results of  $^1H$  NMR spectroscopic investigations of the compounds  $Sb(pyS)_xPh_{3-x}$  ( $x = 3-0$ ) suggest the  $Ph$  protons in *ortho* position to be incorporated into intramolecular  $C-H \cdots S$  contacts for  $x = 2$  and 1. Natural localized molecular orbital (NLMO) calculations were employed in order to gain insights into the electronic situations of the  $Pn$  atoms and  $Pn-R$  bonds ( $R = S, C$ ), especially for the effects caused by formal substitution of  $Pn$  in the compounds  $Pn(pyS)_3$  and the ligand patterns in the compounds  $Sb(pyS)_xPh_{3-x}$  ( $x = 3-0$ ). For the latter series of compounds, the electronic situation of the  $Sb$  atom was further studied by  $^{121}Sb$  Mössbauer spectroscopy, providing a correlation between the calculated electron density at  $Sb$  [ $\rho(0)$ ] and the experimentally observed isomer shift  $\delta$ . The missing link between group 15 and group 13 metal compounds of the type  $M(pyS)_3$ , compound  $Al(pyS)_3$ , was synthesized in this work. In the solid state (confirmed crystallographically), the *mer* isomer of this *tris*-chelate complex with distorted octahedral  $Al$  coordination sphere was found. This coordination mode was confirmed for the solution state ( $CDCl_3$ ) by  $^1H$  and  $^{13}C$  NMR spectroscopy at  $T = -40$  °C.

**Keywords:** Mössbauer spectroscopy; pnictogens; pyridine-2-thiolate; quantum chemical calculations; X-ray diffraction.

\*Corresponding author: Jörg Wagler, Institut für Anorganische Chemie, Technische Universität Bergakademie Freiberg, Leipziger Straße 29, 09596 Freiberg, Germany, E-mail: joerg.wagler@chemie.tu-freiberg.de

Erik Wächtler, Institut für Anorganische Chemie, Technische Universität Bergakademie Freiberg, Leipziger Straße 29, 09596 Freiberg, Germany

Robert Gericke, Institut für Anorganische Chemie, Technische Universität Bergakademie Freiberg, Leipziger Straße 29, 09596 Freiberg, Germany; and School of Chemistry, Trinity College Dublin, 152–160 Pearse Street, Dublin 2, Ireland

Theresa Block, Birgit Gerke and Rainer Pöttgen, Institut für Anorganische und Analytische Chemie, Universität Münster, Corrensstraße 30, 48149 Münster, Germany

**Dedicated to:** In memory of Professor Edwin Weber who was a great teacher of organic chemistry.

## 1 Introduction

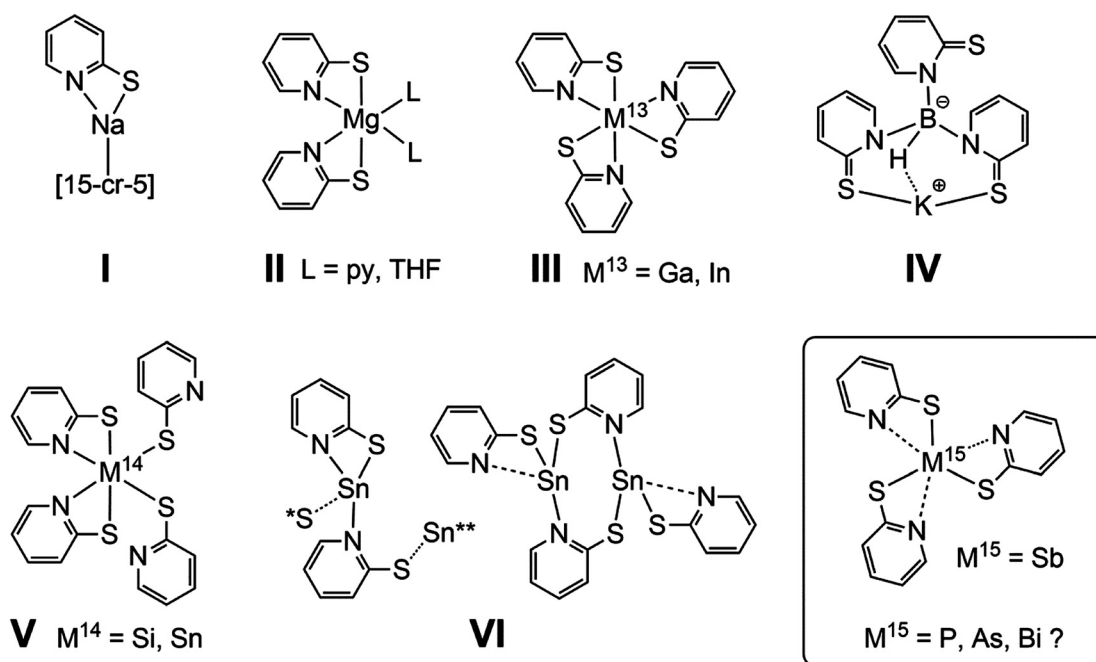
The combination of hard (N) and soft (S) donor atoms as well as the bent  $N-C-S$  motif enables the pyridine-2-thiolate anion ( $pyS^-$ ) to adopt a variety of coordination modes both in transition metal (*TM*) and main group metal or metalloid (*M*) chemistry, e.g. chelating ( $\kappa^2$ -S,N), bridging ( $\mu$ -S,N or  $\mu$ -S), or monodentate ( $\kappa$ -S,  $\kappa$ -N). Several Pd and Pt

complexes featuring the pyS ligand were synthesized which show  $\kappa^2$ -S,N versus  $\kappa$ -S ligand scrambling of two pyS ligands [1], or adopt dinuclear paddle wheel-shaped structures [2]. Unusual eightfold coordination was reported for the mononuclear homoleptic complexes  $TM^4(pyS)_4$  ( $TM^4 = Ti, Zr$ ) [3]. In general, the coordination chemistry of this ligand system in transition metal chemistry has already been extensively studied [4].

In main group metal chemistry, the literature covers some examples of X-ray diffraction studies of the structures of homoleptic pyS compounds, or complexes featuring additional neutral ligands (for alkali and alkaline earth metals) for the completion of the coordination sphere. In this regard, the crown ether complexes of the Li, Na, and K salts of  $pyS^-$  have been isolated and structurally characterized, revealing chelating ( $\kappa^2$ -S,N) or unusual  $\mu$ -S,N-bridging  $pyS^-$  coordination (Scheme 1, e.g. Na( $pyS$ ) [15-Crown-5], **I**) [5]. The  $\kappa^2$ -S,N mode was observed for the Mg complexes Mg( $pyS$ )<sub>2</sub>(L)<sub>2</sub> (**II**; L = THF, py) [6, 7], while the compounds of the type  $M^{13}(pyS)_3$  (**III**;  $M^{13} = In, Ga$ ) feature hexacoordinate metal centers with three  $\kappa^2$ -S,N chelating pyS ligands [8–10]. As other examples of  $pyS^-$  containing  $M^{13}$  compounds, the Na and K salts of the borates BH<sub>2</sub>( $pyS$ )<sub>2</sub><sup>-</sup> [11] and BH( $pyS$ )<sub>3</sub><sup>-</sup> (**IV**) [12], respectively, should be mentioned. Their anions feature monodentate  $\kappa$ -N coordination toward the boron atom and, due to the dangling sulfur atom, they can further be applied in salt elimination reactions for the synthesis of metal complexes *via*  $TM$ -S coordination [13–15]. Based upon the initial report on

the structure of Sn( $pyS$ )<sub>4</sub>·pySH [16], we have recently presented the structures of the homoleptic compounds  $M^{14}(pyS)_4$  (**V**,  $M^{14} = Si, Sn$ ; two chelating, two  $\kappa$ -S-bound pyS ligands) and Sn( $pyS$ )<sub>2</sub> (**VI**, with dimeric and polymeric structures in the solid state) [17]. The investigations on the coordination chemistry of the  $pyS^-$  anion in the coordination sphere of Si by Tacke yielded complexes which are not homoleptic [18]. Lead(II) complexes have been structurally characterized for pyS ligands featuring –CF<sub>3</sub> [19] or –SiMe<sub>3</sub> [20] substituents in 3-position of the pyridine ring, however, the solid state structure of the parent complex Pb( $pyS$ )<sub>2</sub> is unknown. In the last years, we became interested in the compounds Sb( $pyS$ )<sub>3</sub> and Sb( $pyS$ )<sub>2</sub>Ph as we have applied them as ligands for Rh [21] and Pt [22] complexes. In these  $TM$ -Sb complexes, two pyS ligands bridge the  $TM$ -Sb core and, as a result of the charge delocalization within the anionic ligand, a variety of different coordination modes of Sb are accessible. In these cases, the question arose as to whether the  $TM$ -Sb bonds should be referred to as covalent or dative. Related studies focused on the structures of similar  $TM$ - $M^{14}$  ( $M^{14} = Ge, Sn$ ) complexes [23–27] or on a series of  $TM$ -Sb complexes [28, 29] with the oxygen analogue of pyS, *i.e.* 2-pyridyloxy in the  $\mu$ -O,N bridging mode.

Therefore a whole library of the compounds of the type  $M^{15}(pyS)_3$  ( $M^{15} = \text{pnictogen } Pn = P, As, Sb, Bi$ ) appears to be available as starting materials for the syntheses of heterometallic complexes. Except for the crystal and molecular structures of Sb( $pyS$ )<sub>3</sub> (determined by single-crystal X-ray



**Scheme 1:** Compounds I–VI as examples of main group metal or metalloid compounds featuring the pyS ligand.



within the crystal structure can be neglected for the discussion of the metrical parameters of these  $Pn(\text{pyS})_3$  molecules (Table 2). The  $Pn$  atoms are located on a special position (Wyckoff position 12c) and therefore, the asymmetric unit consists of a third of a  $Pn(\text{pyS})_3$  molecule. The molecular structure of  $\text{As}(\text{pyS})_3$  is depicted as an example in Figure 1 (left). The pyS ligands are  $\kappa$ -S-bound to the  $Pn$  central atom in a trigonal pyramidal fashion ( $S-Pn-S$  ca.  $90^\circ$ ). The N atoms point toward  $Pn$ , resulting in a [3+3] pseudo-octahedral coordination and in somewhat longer  $Pn-S$  bonds compared to those in the corresponding pnictogen benzenethiolates ( $Pn(\text{SPh})_3$ :  $Pn = P$ : 2.12 [40]; As: 2.24 [41]; Sb: 2.42 Å [42];  $Pn(\text{pyS})_3$ :  $Pn = P$ : 2.16; As: 2.28; Sb: 2.47 Å). Due to the increasing atomic radii of  $Pn$ , the  $Pn-S$  bond lengths increase in the order  $P < \text{As} < \text{Sb}$ , but the  $S-Pn-N$  angles decrease ( $Pn = P$ :  $62.3^\circ$ ; As:  $61.6^\circ$ ; Sb:  $59.3^\circ$ ). The  $Pn-N$  distances are similar for all three compounds ( $P$ : 2.85; As: 2.82; Sb: 2.84 Å) which is a result of the interplay of two effects: The atomic radii of  $Pn$  increase, leading to longer bonds; with higher atomic number, the tendency of  $Pn$  to adopt higher coordination numbers rises (stronger  $Pn-N$  interactions). The order of the decreasing  $S-Pn-S$  angles  $P (93.7^\circ) > \text{As} (91.7^\circ) > \text{Sb} (89.9^\circ)$  is in accord with VSEPR theory as the electronegativity of  $Pn$  decreases in the same order and the  $Pn-S$  bond electron pairs are shifted toward the S atoms. The same observation was made for the  $Pn(\text{SPh}_3)_3$  compounds, even though the  $S-Pn-S$  angles in these compounds are significantly larger (due to the absence of N- $Pn$  interactions). A very interesting feature of the packing of the  $Pn(\text{pyS})_3$  ( $Pn = P, \text{As}, \text{Sb}$ ) molecules, which has briefly been mentioned for the structure of  $\text{Sb}(\text{pyS})_3$  [30], is the occurrence of pairs of monomers within the crystal structure (selected metrical parameters Table 2). For these pairs, short  $Pn \cdots Pn$  separations are observed ( $Pn = P$ : 3.84; As: 3.64; Sb: 3.66 Å, Figure 1, middle) which are below the sum of the van-der-Waals radii of the  $Pn$  atoms ( $P$ : 3.90; As: 4.10; Sb: 4.40 Å [43]). Intermolecular  $\pi-\pi$  stacking interactions of the pyS ligands within the dimers (Figure 1, right) stabilize this aggregation. The distances of the centroids of the pyridine hexagons ( $P$ : 3.56; As: 3.56; Sb: 3.65 Å) indicate significant non-covalent interactions of the heterocycles. The shortest  $Pn \cdots Pn$  separation can be found for  $Pn = \text{As}$ , indicating a pronounced interaction of the larger pnictogen (As and Sb) with an enhanced tendency toward dispersion interactions in comparison to the P derivative. The poor solubility of the As derivative (in chloroform and THF, *vide supra*) and the higher melting point (approx.  $220^\circ\text{C}$  in this work;  $201-204^\circ\text{C}$  in ref. [33]) in comparison to  $\text{P}(\text{pyS})_3$  (approx.  $120^\circ\text{C}$ ) and  $\text{Sb}(\text{pyS})_3$  (approx.  $205^\circ\text{C}$  this work;  $193^\circ\text{C}$  in ref. [30]) is also indicative of the more pronounced attractive forces between two  $Pn(\text{pyS})_3$  molecules for  $Pn = \text{As}$ .

The solubility of the compound  $\text{Bi}(\text{pyS})_3$  is very poor. Small amounts can be recrystallized *e.g.* from boiling *iso*-butyl methyl ketone or by slow evaporation of a saturated chloroform solution. The crystals obtained by these methods reveal a needle-shaped habitus and are split. The best crystal quality was obtained by slow evaporation (over a period of 10 days at room temperature) of a chloroform solution (15 mL) to which was added a small amount (2 mL) of *iso*-butanol. However, the crystals were twinned, and the data collection and their processing, and the structure solution and refinement were challenging (for details see Supplementary Material available online). Nevertheless, the structure could be solved and refined reasonably well, revealing  $\text{Bi}(\text{pyS})_3$  to crystallize in the monoclinic space group  $Cc$  with cell parameters close to the hexagonal crystal system (Table 1).

The asymmetric unit consists of one  $\text{Bi}(\text{pyS})_3$  molecule featuring two chelating and one  $\kappa$ -S-bound ligands. The N atom of the latter is coordinated to the Bi atom of another molecule, leading to a  $[\text{Bi}(\kappa^2\text{-S}, \text{N-pyS})_2(\mu\text{-S}, \text{N-pyS})]_n$  polymer chain (along the crystallographic  $b$  axis) with  $\text{Bi} \cdots \text{Bi}$  van-der-Waals contacts and a total coordination number of the pnictogen atom of 6 (see Figure 2 for graphical representation and Table 2 for metrical parameters). The coordination geometry of the Bi atom can neither be described as regular octahedral nor as trigonal prismatic. Three Bi-S bonds are arranged trigonal pyramidally with  $S-\text{Bi}-S$  angles close to  $90^\circ$  ( $87-90^\circ$ ), similar to the other  $Pn(\text{pyS})_3$  compounds ( $Pn = P, \text{As}, \text{Sb}$ ) with Bi-S bond lengths of 2.70–2.74 Å. The Bi-N bond lengths of the chelating pyS ligands (2.66, 2.69 Å) are shorter than in the other  $Pn(\text{pyS})_3$  derivatives (featuring  $\kappa$ -S-bound pyS ligands with only weak  $Pn \cdots \text{N}$  contacts) and also than the third Bi-N bond (2.76 Å). The N-Bi-N angles are found in a quite narrow range (with N atoms in the Bi core environment, involving N atoms of other asymmetric units;  $113-122^\circ$ ) compared to the *trans* S-Bi-N angles which are in a wider range ( $139-162^\circ$ ). Considering the Bi atom to be located within the planes spanned by the three N atoms in direct environment and by the three S atoms, the heavy pnictogen atom is shifted out of the  $\text{N}_3$  plane by only 0.20 Å, compared to 1.62 Å from the  $\text{S}_3$  plane (opposite direction). Hence, the coordination environment is rather asymmetrical, suggesting the presence of a stereochemically active lone pair. Alignment of the Bi atoms along a chain with bridging of the  $\text{Bi} \cdots \text{Bi}$  contacts by one pyS ligand per Bi atom, and the absence of symmetry elements within the  $\text{Bi}(\text{pyS})_3$  moieties arising therefrom, give rise to this acentric unit cell setting. The polymeric structure observed for  $\text{Bi}(\text{pyS})_3$  is in contrast to the monomeric structure found for the trimethylsilyl derivative  $\text{Bi}(2\text{-S-C}_5\text{H}_3\text{N-3-SiMe}_3)_3$  (Bi-S: 2.54–2.65 Å; Bi-N:

**Table 1:** Crystal data and parameters of data collection and structure refinement for the structures of  $Pn(\text{pyS})_3$  ( $Pn = \text{P, As, Bi}$ ) and  $\text{Al}(\text{pyS})_3 \cdot 0.5(\text{C}_7\text{H}_8)$ .

	$\text{P}(\text{pyS})_3$	$\text{As}(\text{pyS})_3$	$[\text{Bi}(\kappa^2\text{-S,N-pyS})_2(\mu\text{-S,N-pyS})_n]$	$\text{Al}(\text{pyS})_3 \cdot 0.5(\text{C}_7\text{H}_8)$
Chemical formula	$\text{C}_{15}\text{H}_{12}\text{N}_3\text{PS}_3$	$\text{C}_{15}\text{H}_{12}\text{AsN}_3\text{S}_3$	$\text{C}_{15}\text{H}_{12}\text{BiN}_3\text{S}_3$	$\text{C}_{37}\text{H}_{32}\text{Al}_2\text{N}_6\text{S}_6$
$M_r$	361.43	405.38	539.44	807.00
Temperature, K	150	150	180	150
Crystal system	trigonal	trigonal	monoclinic	triclinic
Space group	$R\bar{3}c$	$R\bar{3}c$	$Cc$	$P\bar{1}$
$a$ , Å	12.3117(8)	12.3541(3)	21.4670(9)	7.8143(6)
$b$ , Å	$= a$	$= a$	4.1502(1)	9.1858(7)
$c$ , Å	37.292(3)	37.290(1)	21.2141(8)	14.5011(11)
$\alpha$ , deg	90	90	90	81.122(6)
$\beta$ , deg	90	90	120.784(3)	87.660(6)
$\gamma$ , deg	120	120	90	68.539(6)
$V$ , Å <sup>3</sup>	4895.4(7)	4928.9(3)	1623.7(1)	956.98(13)
$Z$	12	12	4	1
$F(000)$ , $e$	2232	2448	1016	418
$D_x$ , g cm <sup>-3</sup>	1.47	1.64	2.21	1.40
$\mu$ , mm <sup>-1</sup>	0.6	2.5	11.2	0.4
Crystal size, mm <sup>3</sup>	$0.40 \times 0.40 \times 0.25$	$0.45 \times 0.40 \times 0.35$	$0.60 \times 0.03 \times 0.02$	$0.25 \times 0.20 \times 0.10$
$T_{\text{min}}/T_{\text{max}}$	0.972/0.991	0.802/0.945	0.009/0.030	0.898/0.957
Measured reflections	6993	18254	41664	14901
Unique reflections	1903	1910	41664	5566
Observed reflections with $ I  > 2\sigma(I)$	1685	1806	27653	4439
$R_{\text{int}}$	0.033	0.064	–	0.039
$\theta$ values, deg	2.9–32.0	2.9–32.0	3.8–28.5	2.9–30.0
$(\sin \theta/\lambda)_{\text{max}}$ , Å <sup>-1</sup>	0.746	0.745	0.671	0.704
Range of $h, k, l$	$h = -18 \rightarrow 17$ $k = -18 \rightarrow 10$ $l = -49 \rightarrow 54$	$h = -18 \rightarrow 18$ $k = -17 \rightarrow 18$ $l = -54 \rightarrow 54$	$h = -28 \rightarrow 28$ $k = -5 \rightarrow 5$ $l = -28 \rightarrow 28$	$h = -10 \rightarrow 9$ $k = -12 \rightarrow 11$ $l = -20 \rightarrow 20$
No. of reflections	1903	1910	41664	5566
No. of ref. parameters	67	67	202	245
No. of restraints	0	0	20	1
$R [F^2 > 2\sigma(F^2)]$	0.032	0.024	0.044	0.040
$wR(F^2)$	0.082	0.064	0.133	0.087
$S$	1.09	1.11	1.09	1.05
$(\Delta/\sigma)_{\text{max}}$	0.002	0.001	<0.001	0.001
Flack $x^a$	–	–	-0.032(8)	–
$\Delta\rho_{\text{max}}/\Delta\rho_{\text{min}}$ , e Å <sup>-3</sup>	0.41/-0.29	0.83/-0.46	2.11/-1.96	0.52/-0.41

<sup>a</sup>Absolute structure parameter.**Table 2:** Selected  $Pn\text{-R}$  bond lengths (Å),  $\text{R-Pn-R}$  bond angles (deg) ( $\text{R} = \text{S, N}$ ), distances of  $Pn \cdots Pn$  contacts (Å) in comparison to the two-fold van-der-Waals radius  $r_{\text{vdW}}$  (Å) of  $Pn$ , and distances between the centroids  $\text{CE}$  (Å) of the pyS ligands for the compounds  $Pn(\text{pyS})_3$  ( $Pn = \text{P, As, Sb}$ ) and selected parameters for  $\text{Bi}(\text{pyS})_3$ .

$Pn$	$Pn\text{-S}$	$Pn \cdots N$	$\text{S-Pn-S}$	$\text{S-Pn-N}^a$	$Pn \cdots Pn$	$2r_{\text{vdW}}^b$	$\text{CE} \cdots \text{CE}$
P	2.1564(4)	2.853(1)	93.72(2)	62.29(2)	3.843(1)	3.60	3.56
As	2.2840(3)	2.816(1)	91.70(1)	61.62(2)	3.643(1)	3.70	3.56
Sb <sup>c</sup>	2.470(1)	2.837(3)	89.86(4)	59.33(6)	3.663(1)	4.12	3.65
Bi	2.71 <sup>d</sup> 2.738(7) <sup>e</sup>	2.68 <sup>d</sup> 2.76(2) <sup>f</sup>	88 <sup>g</sup>	58 <sup>a,d</sup>	4.150(1) <sup>h</sup>	4.14	–

<sup>a</sup>S and N atoms of the same pyS ligand; <sup>b</sup>van-der-Waals radii taken from ref. [43]; <sup>c</sup>ref. [31]; <sup>d</sup>average from the two similar chelating pyS ligands; <sup>e</sup>to  $\kappa\text{-S}$ -bound ligand; <sup>f</sup>dative bond to  $\kappa\text{-S}$ -bound ligand of another monomeric unit; <sup>g</sup>average from three similar angles; <sup>h</sup>the  $\text{Bi} \cdots \text{Bi}$  distance equals the length of the crystallographic  $b$  axis.

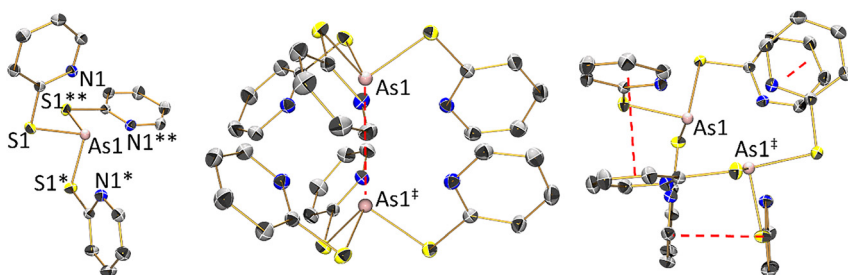


**Figure 1:** Molecular structure of  $\text{As}(\text{pyS})_3$  in the crystal. Ellipsoids set at the 50% probability level and hydrogen atoms omitted for clarity. Left:  $\text{As}(\text{pyS})_3$  molecule. Middle:  $Pn \cdots Pn$  contacts between two molecules highlighted with red dashed line. View along  $[100]$ . Right:  $\pi$ - $\pi$  stacking between two  $\text{pyS}$  ligands highlighted with red dashed line. Symmetry operations:  $1+y-x, 1-x, z$  (\*),  $1-y, -y+x, z$  (\*\*), threefold rotational axis;  $x, y, 0.5-z$  (‡),  $c$  glide plane + sixfold rotation-inversion.

2.69–2.83 Å) in which the enhanced steric bulk of the ligands does not allow for a close proximity of the ligands [31]. Regarding  $\text{pyS}$ -containing  $\text{Bi}(\text{III})$  compounds, a polymeric structure was also found for  $[\text{Bi}(\kappa^2\text{-S,N}, \mu\text{-S-pyS})_2]_n$  ( $\text{Bi-S}$ : 2.86–2.93 Å;  $\text{Bi-N}$ : 2.55) [44].

Due to the fact that  $\text{Ph/pyS}$  mixed substituted pnictogen compounds are also interesting starting materials for the syntheses of  $TM$  complexes (see ref [22]), we studied the series of  $\text{Sb}(\text{pyS})_x\text{Ph}_{3-x}$  compounds ( $x = 3-0$ ;  $x = 3$  *vide supra*;  $x = 0$  commercially available and well-studied). This study could give comparative insights into the state of bonding of the  $Pn$  atoms with varying substitution patterns, which in case of this pnictogen can also be experimentally assessed using  $^{121}\text{Sb}$  Mössbauer spectroscopy. Whereas  $\text{Sb}(\text{pyS})\text{Ph}_2$  had not previously been described, the synthesis of  $\text{Sb}(\text{pyS})_2\text{Ph}$  [starting from  $\text{SbCl}_2\text{Ph}$  and  $\text{Na}(\text{pyS})$ ] was briefly reported and the crystal structure of the product determined, but with lack of details of the experimental procedure and incomplete characterization [33].  $\text{SbCl}_2\text{Ph}$  and  $\text{SbClPh}_2$  can be prepared through the reactions of  $\text{SbCl}_3$  with  $\text{SbPh}_3$  in a 2:1 or 1:2 ratio, respectively [45]. However, these reactions do not afford pure products, with  $\text{SbCl}_2\text{Ph}$  e.g. being contaminated with

$\text{SbClPh}_2$  and unreacted  $\text{SbCl}_3$ . Upon attempted  $\text{pyS}$  substitution (using  $\text{NEt}_3$  as supporting base) in THF, we found these impurities to cause significant problems regarding crystallization and isolation of the final products as  $\text{Sb}(\text{pyS})_3$  and  $\text{Sb}(\text{pyS})_2\text{Ph}$  have similar solubilities (and this is also true for the pair of  $\text{SbPh}_3$  and  $\text{Sb}(\text{pyS})\text{Ph}_2$ ). Facing this issue, we have developed a synthetic protocol for the reaction of  $\text{SbCl}_3$  and  $\text{SbPh}_3$  in a 1:1 ratio. Along this route, the amounts of remaining  $\text{SbCl}_3$  and  $\text{SbPh}_3$  in the  $\text{SbCl}_2\text{Ph/SbClPh}_2$  mixture are reduced to a minimum, and upon  $\text{pyS}$  for  $\text{Cl}$  substitution both  $\text{Sb}(\text{pyS})_2\text{Ph}$  and  $\text{Sb}(\text{pyS})\text{Ph}_2$  are obtained which can easily be separated by workup in hot hexane (solubility of the latter). This facile procedure gave  $\text{Sb}(\text{pyS})_2\text{Ph}$  and  $\text{Sb}(\text{pyS})\text{Ph}_2$  in good yields and purity (Scheme 3).

Unfortunately, the crystals obtained for  $\text{Sb}(\text{pyS})\text{Ph}_2$  were only of poor quality and did not allow for X-ray structure determination. Hence, we have optimized the molecular structure of this compound by quantum chemical methods (see Supplementary Material available online). Even though a comparison of the calculated structure of this compound (in vacuum) with the crystallographically determined structures of related compounds is,

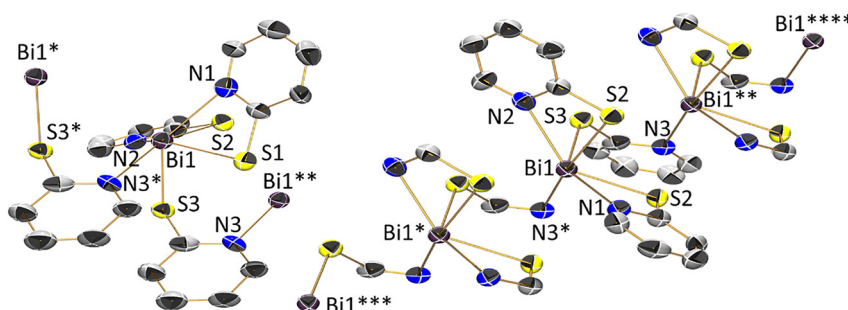
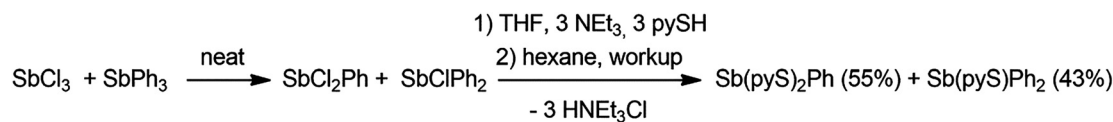


**Figure 2:** Two representations of the molecular structure of the  $\text{Bi}(\text{pyS})_3$  coordination polymer; left: direct coordination environment of the  $\text{Bi}$  atom, including the  $\kappa\text{-S-pyS}$  ligand of another molecule as well as two symmetry equivalent  $\text{Bi}$  atoms; right: chain of five  $\text{Bi}(\text{pyS})_3$  molecules along the crystallographic  $b$  axis with the  $\text{pyS}$  ligands outside the central asymmetric unit being reduced to the  $\text{N-C-S}$  atoms for clarity. Ellipsoids set on the 50% level and hydrogen atoms omitted. Symmetry operations:  $x, y-1, z$  (\*);  $x, y+1, z$  (\*\*);  $x, y-2, z$  (\*\*\*) ;  $x, y+2, z$  (\*\*\*\*); translations along the  $b$  axis.



**Scheme 3:** One-pot synthesis of the compounds  $\text{Sb(pyS)}_2\text{Ph}$  and  $\text{Sb(pyS)Ph}_2$ .

strictly speaking, not meaningful in terms of bond lengths and angles, we include this structure into the comparative discussion because the optimized structure of  $\text{Sb(pyS)Ph}_2$  is in accord with the general trends observed. The molecular structures of the compounds  $\text{Sb(pyS)}_x\text{Ph}_{3-x}$  ( $x = 3-0$ ; 3 ref. [30, 31], 2 ref. [32], 0 ref. [46]) are depicted in Figure 3, and the metrical parameters are summarized in Table 3. The trigonal pyramidal  $\text{SbS}_2\text{C}$  motif in the structure of  $\text{Sb(pyS)}_2\text{Ph}$  is capped by the two N atoms in a way that they donate electron density toward the  $\text{Sb-S } \sigma^*$  orbitals. As a result, the pyS ligands and the Sb atom are located almost within a common plane. Due to the lower coordination number ([2+3] coordination), the  $\text{Sb}\cdots\text{N}$  contacts (2.63; 2.73 Å) of this compound are shorter than in  $\text{Sb(pyS)}_3$  (2.84 Å; [3+3] coordination). The donation of lone pair electron density from N toward the  $\text{Sb-S } \sigma^*$  orbital is not possible in  $\text{Sb(pyS)Ph}_2$ , ( $\text{Sb-N}$  separation 2.92 Å). The sum of the  $\text{R-Sb-R}$  angles ( $\text{R} = \text{S, C}$ ) increases with the number of phenyl groups.

## 2.2 NMR spectroscopy

The proton NMR spectra of the compounds  $\text{Pn(pyS)}_3$  ( $\text{Pn} = \text{P, As, Sb, Bi}$ ) were recorded in  $\text{CDCl}_3$ , even though the As and Bi compounds exhibit only very poor solubility. The spectra show one set of signals of the four protons of the pyS ligand (Figure 4; the proton and carbon atoms are labeled according to Hantzsch/Widman with the positions  $\text{N}^1\text{-C}^2=\text{S}-(\text{C}^3\text{-H}^3)-(\text{C}^4\text{-H}^4)\dots$ ; [47, 48]). The Bi compound shows an averaged set of signals for the pyS ligands due to the fast exchange between different pyS coordination modes in solution (e.g. chelating and  $\kappa\text{-S}$  bound) on the

**Table 3:** Sb-S and Sb-C bond lengths (Å),  $\text{Sb}\cdots\text{N}$  distances (Å) and sum of the three  $\text{R-Sb-R}$  ( $\text{R} = \text{S, C}$ ) angles (deg) of the compounds  $\text{Sb(pyS)}_x\text{Ph}_{3-x}$  ( $x = 3-0$ ).

Compound	Sb-S	Sb-C	Sb...N	$\Sigma(\text{R-Sb-R})$
$\text{Sb(pyS)}_3^{\text{a}}$	2.47	/	2.84	269.6
$\text{Sb(pyS)}_2\text{Ph}^{\text{b}}$	2.50/2.50	2.16	2.63/2.73	276.5
$\text{Sb(pyS)Ph}_2^{\text{c}}$	2.49	2.18/2.19	2.92	286.7
$\text{SbPh}_3^{\text{d}}$	-	2.14-2.15	-	289.0

<sup>a</sup>Ref. [31]; <sup>b</sup>ref. [32]; <sup>c</sup>Molecular structure optimized in vacuum; <sup>d</sup>ref. [46].

NMR time scale. The multiplet signals of the pyS ligand protons (i.e. ddd patterns) could in most cases be resolved and assigned. Due to the adjacent N atom, the  $\text{H}^6$  proton resonance is shifted downfield (>8 ppm) and the  $^3J_{\text{H-5/H-6}}$  coupling constant is reduced (around 5 Hz; 7–8 Hz for other  $^3J_{\text{H-H}}$ ). The change of the  $\text{Pn}$  atom leads to an up-field shift of all signals in the order of  $\text{Pn} = \text{P, As, Sb}$ . However, the Bi compound does not follow this trend which might either be explained by the different (averaged) pyS coordination or the contribution of relativistic effects to the chemical shift in case of this heavy atom.

Caused by the poor solubility of the As and Bi compounds,  $^{13}\text{C}\{^1\text{H}\}$  CP/MAS NMR spectra of the solids were recorded (Figure 5). In accord with the molecular structures in the crystal, the former reveals one set of pyS signals, whereas the different coordination modes of the pyS ligands in  $\text{Bi(pyS)}_3$  lead to the detection of a complex set of signals.

The solution  $^{31}\text{P}\{^1\text{H}\}$  NMR spectroscopic investigation of  $\text{P(pyS)}_3$  reveals a signal at 91 ppm. Due to the shielding caused by the  $\text{N}\cdots\text{P}$  contacts, this signal is significantly more up-field shifted compared to that of  $\text{P(SPh}_3)$  (131 ppm)

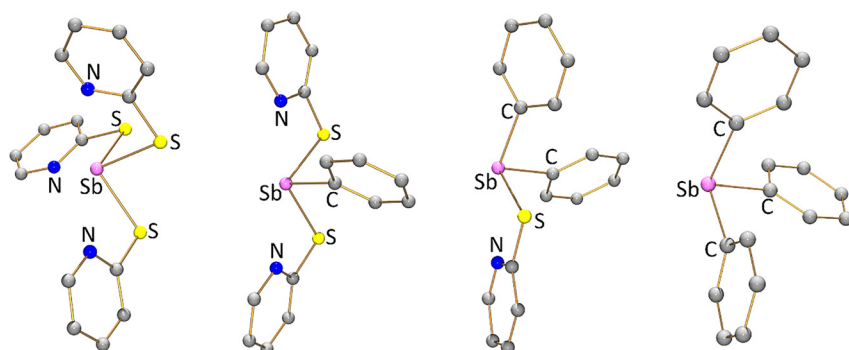


**Figure 3:** Molecular structures of the compounds  $\text{Sb(pyS)}_x\text{Ph}_{3-x}$  ( $x = 3$ : ref. [31]; 2: ref. [32]; 1: molecular structure optimized in vacuum; 0: ref. [46]).

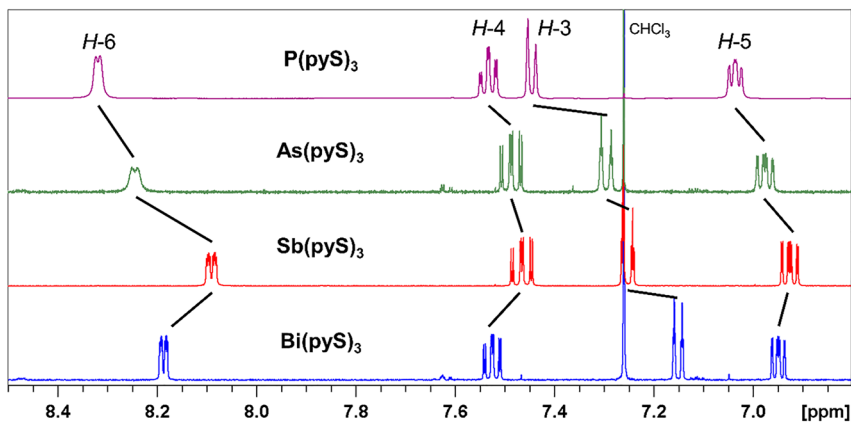


Figure 4:  $^1\text{H}$  NMR spectra of the compounds  $Pn(\text{pyS})_3$  ( $Pn = \text{P-Bi}$ ) in  $\text{CDCl}_3$ .

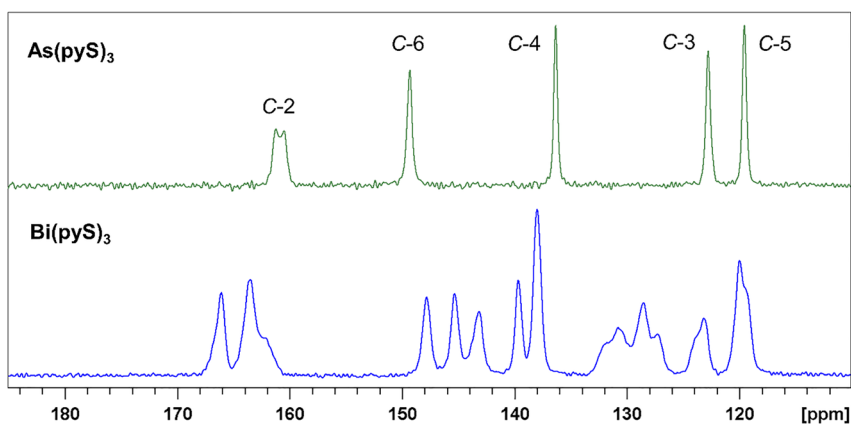


Figure 5:  $^{13}\text{C}\{^1\text{H}\}$  CP/MAS NMR spectra ( $\nu_{\text{rot}} = 10$  kHz) of  $\text{As}(\text{pyS})_3$  and  $\text{Bi}(\text{pyS})_3$ .

[49]. In the NMR spectra of the compounds  $\text{Sb}(\text{pyS})_x\text{Ph}_{3-x}$  ( $x = 3-0$ ; Figure 6), the most pronounced effect is the down-field shift of the *ortho*-proton resonance of the Ph substituents with increasing  $x$ .  $\text{CH}\cdots\text{S}$  contacts with the pyS ligands, which should in general be accompanied by a down-field shift, are the most likely cause [50].

### 2.3 NLMO calculations

Natural localized molecular orbital (NLMO) calculations of the compounds  $Pn(\text{pyS})_3$  ( $Pn = \text{P, As, Sb, Bi}$ ) and  $\text{Sb}(\text{pyS})_x\text{Ph}_{3-x}$  ( $x = 3-0$ ) were performed in order to elucidate the changes of the bonding characteristics of the  $Pn$  atoms induced by replacing the  $Pn$  atoms or modifying their ligand patterns. The electronic structure of the Bi atom within the coordination polymer was accessed by the calculation of a trimeric model  $[\text{Bi}(\text{pyS})_3]_3$ , for which the data of the central Bi atom is given and discussed. The NLMO analyses indicate the presence of  $Pn$  lone pairs (LP-NLMOs) with predominant  $s$ -orbital character and  $Pn$ -S and Sb-C bonds (BD-NLMOs) with a predominant  $p$ -orbital contribution of  $Pn$  (Table 4). This is in good agreement with the general observation of trigonal pyramidal  $Pn\text{S}_3$  units (featuring S- $Pn$ -S angles

close to  $90^\circ$ ). For the pnictogen thiolates, the increasing difference in electronegativity between  $Pn$  and S causes the  $Pn$ -S BD-NLMO to be shifted toward S for the heavier pnictogen (%  $Pn$ /% S contribution: P 38/60; As 34/65; Sb 27/71; Bi 19/77 av.). This is also reflected by the increasing natural charges (NC, Table 5) of  $Pn$  (P 0.56; As 0.80; Sb 1.14; Bi 1.30 e), which is mainly a result of a decreasing  $p$ -orbital population ( $N_p$ , P 2.62; As 2.35; Sb 2.01; Bi 1.71 e), in contrast to a slight increase in  $s$ -orbital population ( $N_s$ , P 1.75; As 1.83; Sb 1.84; Bi 1.94 e) of  $Pn$ . Regarding the  $s$  and  $p$ -orbital contributions toward the  $Pn$ -S BD-NLMO, there is a noticeable tendency toward an increasing  $s$ -orbital contribution to the  $Pn$  LP-NLMO (%  $s$ /%  $p$ : P 79/21; As: 88/12; Sb: 89/11; Bi: 97/3) and an increasing  $p$ -orbital contribution to the  $Pn$ -S BD-NLMOs (%  $s$ /%  $p$ : P: 8/91; As, Sb: 5/95; 1/98), like it is typically found in main group chemistry. For the compounds  $\text{Sb}(\text{pyS})_x\text{Ph}_{3-x}$  ( $x = 3-0$ ), the similar electronegativities of C and S are reflected by comparable contributions of these atoms toward the Sb-R bonds (R = C: 69–70%; R = S: 70–72%; Sb contribution: 25–28%). However, significant differences can be found for the  $s$  and  $p$ -orbital contribution of Sb toward the Sb-R bonds: For the larger S atoms (and hence longer Sb-R bonds), more favorable orbital overlaps are realized with high  $p$ -orbital contributions of Sb (5–8%  $s$ ;

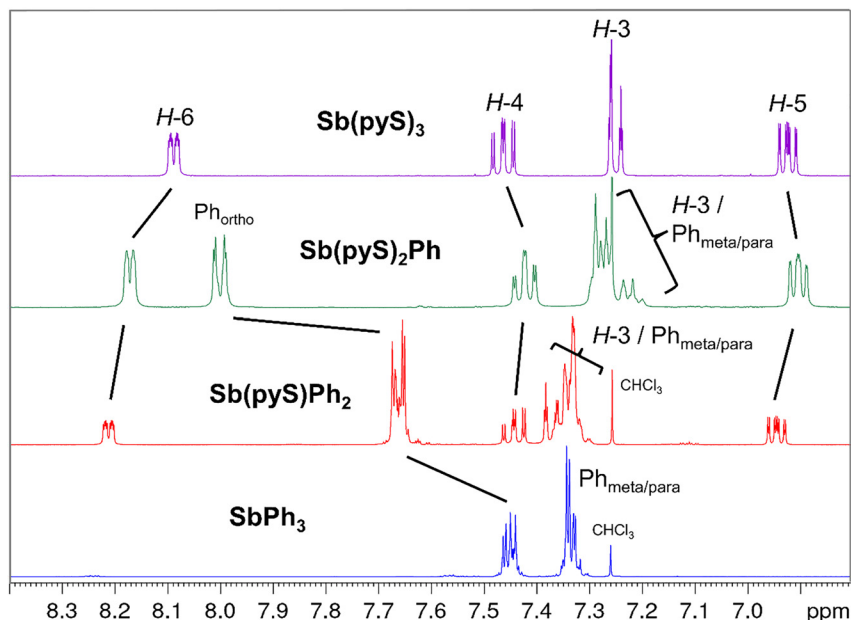


Figure 6:  $^1\text{H}$  NMR spectra of compounds  $\text{Sb}(\text{pyS})_x\text{Ph}_{3-x}$  ( $x = 3-0$ ) in  $\text{CDCl}_3$ .

92–95%  $p$ ) and S (12–14%  $s$ ; 86–88%  $p$ ), whereas for  $R = \text{C}$  the  $s$  character of the  $\text{Sb}-\text{R}$  bonds is increased (Sb: 11–13%  $s$ ; 87–89%  $p$ ; C: 25–26%  $s$ ; 74–76%  $p$ ). Thus, for the compounds  $\text{Sb}(\text{pyS})_x\text{Ph}_{3-x}$  ( $x = 3-0$ ) the Sb atoms contribute more  $s$  electron density to their BD-NLMOs with decreasing  $x$ , and therefore the  $p$ -orbital contribution to the Sb LP-NLMO is enhanced (%  $s/\% p$ ,  $x = 3$ : 89/11;  $x = 2$ : 82/18;  $x = 1$ : 77/23;  $x = 0$ : 68/32). This matches well with the observed molecular structures as the sum of  $\text{R}-\text{Sb}-\text{R}$  angles increases with the phenyl content (*vide supra*). The increasing NC of Sb in these compounds ( $x = 3-0$ , 1.14; 1.22; 1.25; 1.29  $e$ ) can be explained by the less effective charge compensation of the harder C donor compared to the softer S donor atom.

Finally, the energies of the  $\text{N} \rightarrow \text{Pn}$  interactions can be determined by second order perturbation theory analysis (Table 4). They are in good agreement with the trends observed for the  $\text{Pn} \cdots \text{N}$  distances (*vide supra*): For the compounds  $\text{Pn}(\text{pyS})_3$ , the energies increase with the growth of the atomic number ( $\text{Pn} = \text{P}$ : 5; As: 9; Sb: 10; Bi: av. 21  $\text{kcal mol}^{-1}$ ), and for the series of  $\text{Sb}(\text{pyS})_x\text{Ph}_{3-x}$  compounds, they decrease in the order of  $x = 2$  (av. 13), 3 (10) and 1 (4  $\text{kcal mol}^{-1}$ ).

## 2.4 Mössbauer spectroscopy

The  $^{121}\text{Sb}$  Mössbauer spectra of the compounds  $\text{Sb}(\text{pyS})_x\text{Ph}_{3-x}$  ( $x = 2-0$ ) were recorded and are depicted in Figure 7 [51–53]. In contrast to  $^{57}\text{Fe}$  or  $^{119}\text{Sn}$  Mössbauer spectroscopy, the mean square radius of the isotope  $^{121}\text{Sb}$  in the ground state is smaller than in the excited state (*i.e.* negative  $\langle \Delta r^2 \rangle$

[54]) and therefore, a reduction of the electron density at the Sb nucleus results in less negative values for the isomer shift  $\delta$  of the signal. The electron density at the Sb nucleus

Table 4: Selected data of the NLMO calculations of the compounds  $\text{Pn}(\text{pyS})_3$  ( $\text{Pn} = \text{P}, \text{As}, \text{Sb}, \text{Bi}$ ) and  $\text{Sb}(\text{pyS})_x\text{Ph}_{3-x}$  ( $x = 3-0$ ): percentage of atomic contributions of  $\text{Pn}$ , S and C atoms to the NLMO for the lone pair (LP) $\text{Pn}$  and bonding (BD) $\text{Pn}-\text{R}$  ( $\text{R} = \text{S}, \text{C}$ ) NLMOs with hybrid composition ratios of the parent natural atomic orbitals (%  $s/\% p$ ) in parentheses, energy  $E$  ( $\text{kcal mol}^{-1}$ ) of the strongest donor acceptor interaction between LP(N) and  $\text{Pn}-\text{S}^*$  calculated by second order perturbation theory analysis.

compound	LP( $\text{Pn}$ )	BD( $\text{Pn}-\text{C}$ )	BD( $\text{Pn}-\text{S}$ )	$E$ ( $\text{N} \rightarrow \text{Pn}$ )
$\text{P}(\text{pyS})_3$	99 P (79/21)	–	38 P (8/91) 60 S (14/86)	5.4
$\text{As}(\text{pyS})_3$	99 As (88/12)	–	34 As (5/95) 65 S (13/86)	8.8
$\text{Sb}(\text{pyS})_3$	99 Sb (89/11)	–	27 Sb (5/95) 71 S (14/86)	10.2
$\text{Bi}(\text{pyS})_3$	99 Bi (97/3)	–	19 Bi (1/98) 78 S (16/84) <sup>a</sup> 20 Bi (1/99) 76 (11/88) <sup>b</sup>	19.1, 20.2 22.6
$\text{Sb}(\text{pyS})_2\text{Ph}$	99 Sb (82/18)	28 Sb (12/88) 70 C (25/75)	25 Sb (5/95) 72 S (13/86)	15.0, 11.3
$\text{Sb}(\text{pyS})\text{Ph}_2$	99 Sb (77/23)	27 Sb (11/89) 70 C (25/74)	28 Sb (8/92) 70 S (12/88)	4.4
$\text{SbPh}_3$	98 Sb (68/32)	28 Sb (13/87) 69 C (26/76)	–	–

<sup>a</sup>Average of the two similar Bi–S bonds to the  $\kappa^2\text{-S,N-pyS}$  ligand; <sup>b</sup>to  $\kappa\text{-S-pyS}$ .

**Table 5:** Natural charges ( $e$ ) and valence shell natural electron configuration ( $e$ ) of the  $Pn$  atoms of the compounds  $Pn(\text{pyS})_3$  ( $Pn = \text{P, As, Sb, Bi}$ ) and  $\text{Sb}(\text{pyS})_x\text{Ph}_{3-x}$  ( $x = 3-0$ ).

	$\text{P}(\text{pyS})_3$	$\text{As}(\text{pyS})_3$	$\text{Sb}(\text{pyS})_3$	$\text{Bi}(\text{pyS})_3$	$\text{Sb}(\text{pyS})_2\text{Ph}$	$\text{Sb}(\text{pyS})\text{Ph}_2$	$\text{SbPh}_3$
NC	0.56	0.80	1.14	1.30	1.22	1.25	1.29
$N_s$	1.75	1.83	1.84	1.94	1.75	1.68	1.56
$N_p$	2.62	2.35	2.01	1.71	2.01	2.06	2.14

$\rho(0)$  (in  $e a_0^{-3}$ ) can be deduced from the  $N_{5s/p}$ -orbital populations by the empirical equation:

$$\rho(0) = 0.11 + 68.65N_{5s} - 3.39N_{5p} - 5.57N_{5s}^2 - 1.00N_{5s}N_{5p} \text{ [55]}$$

The calculated values (derived from the  $N_{5s/p}$  values given in Table 5) are summarized together with the parameters of the data fitting procedure of the  $^{121}\text{Sb}$  Mössbauer spectra in Table 6. The magnitude of  $\rho(0)$  is in the expected range for  $\text{Sb}(\text{III})$  compounds [55] and follows the order  $\text{SbPh}_3 < \text{Sb}(\text{pyS})\text{Ph}_2 < \text{Sb}(\text{pyS})_2\text{Ph} < \text{Sb}(\text{pyS})_3$ . The  $\delta = f[\rho(0)]$  plot (see Supplementary Material available online) gives a good fit with a correlation coefficient of 98%, indicating that the pairs of calculated and measured electron density at the Sb nucleus are in good agreement and thus supporting the validity of the theoretical method applied. For the compounds  $\text{Sb}(\text{pyS})_2\text{Ph}$  and  $\text{Sb}(\text{pyS})\text{Ph}_2$ , the heteroleptic substitution pattern causes larger electronic quadrupole interactions ( $eQV_{ZZ}$ ; 11.2(1) and 10.4(1)  $\text{mm s}^{-1}$ , respectively) and larger asymmetry parameters  $\eta$  [0.41(3), 0.74(3)] in comparison to those of the homoleptic compounds  $\text{Sb}(\text{pyS})_3$  [ $eQV_{ZZ}$  6.1(1)  $\text{mm s}^{-1}$ ] and  $\text{SbPh}_3$  [ $eQV_{ZZ}$  9.3(1)  $\text{mm s}^{-1}$ ], while the slightly larger  $p$ -orbital population, *i.e.* the non-spherical electron density, of the latter also causes an enhanced  $eQV_{ZZ}$  value compared to that of  $\text{Sb}(\text{pyS})_3$ .

## 2.5 Comparison with group 13 analogues

While this study of group 15 compounds  $Pn(\text{pyS})_3$  revealed a systematic trend of increasing tendency toward  $\text{N} \rightarrow Pn$  coordination in the order  $Pn = \text{P, As, Sb, Bi}$ , a similar trend for their group 13 analogues  $M^{13}(\text{pyS})_3$  cannot be derived because of the lack of data for  $\text{Al}(\text{pyS})_3$ . For  $M^{13} = \text{In}$  and  $\text{Ga}$ , octahedral coordination of the group 13 element has been reported, with the three pyS ligands adopting a *fac* configuration [8–10]. In this regard, these two compounds are related to the general  $\text{N} \rightarrow Pn$  coordination motif, where also a *fac* coordination in highly distorted octahedral geometries was observed.

In order to probe whether the smaller Al atom would cause a lowering of the coordination number (or weakening

of the  $\text{N} \rightarrow M^{13}$  interaction), we synthesized  $\text{Al}(\text{pyS})_3$  and determined its crystal structure (see Table 1 and Supplementary Material available online for further details including a plot of the molecular structure in the crystal). In brief, also in  $\text{Al}(\text{pyS})_3$  a chelating coordination mode of all three pyS ligands is encountered. However, the smaller group 13 element Al causes a change of the octahedral coordination from a *fac* to a *mer* configuration. As confirmed by  $^1\text{H}$  and  $^{13}\text{C}$  NMR spectroscopy at  $T = -40^\circ\text{C}$ , this configuration is also favored in  $\text{CDCl}_3$  solution.

## 3 Conclusions

With the results discussed herein, we present the first comprehensive study of the synthesis and detailed analysis (X-ray diffraction, NMR spectroscopy, mp, elemental analysis, NLMO calculations) of the series of homoleptic pnictogen(III) pyridine-2-thiolates  $Pn(\text{pyS})_3$  ( $Pn = \text{P, As, Sb, Bi}$ ), which is also the first report on the phosphorus compound. The phosphorus and arsenic compounds were found to crystallize isostructurally to the structure reported for  $\text{Sb}(\text{pyS})_3$ , for which the presence of molecule pairs featuring  $Pn \cdots Pn$  contacts was already noticed. A comparison of those structures revealed those contacts to be most pronounced for  $Pn = \text{As}$ , which accounts for the higher melting point and lower solubility in comparison with  $Pn = \text{P}$  and  $\text{Sb}$ . The low solubility of  $\text{Bi}(\text{pyS})_3$ , its poor crystal quality and the cell parameters of a monoclinic structure close to the hexagonal crystal system (and heavy twinning associated therewith) hampered the crystallographic determination of this molecular structure. With optimized crystallization conditions, its structure was shown to be that of a  $[\text{Bi}(\kappa^2\text{-S}, \text{N-pyS})_2(\mu\text{-S}, \text{N-pyS})_n]$  coordination polymer featuring two chelating and one  $\kappa\text{-S}$  bound pyS ligands.  $^1\text{H}$  NMR investigations, however, suggest that discrete  $\text{Bi}(\text{pyS})_3$  molecules are present in chloroform solution.

The electronic structures of the compounds  $Pn(\text{pyS})_3$  were investigated by NLMO calculations, which detected lone pair NLMOs with a high degree of  $s$  electron density located at  $Pn$ . The bonding  $Pn\text{-S}$  NLMOs reveal predominant  $p$  character, which is in good agreement with the trigonal pyramidal  $Pn\text{S}_3$  structural motif for all four compounds. In

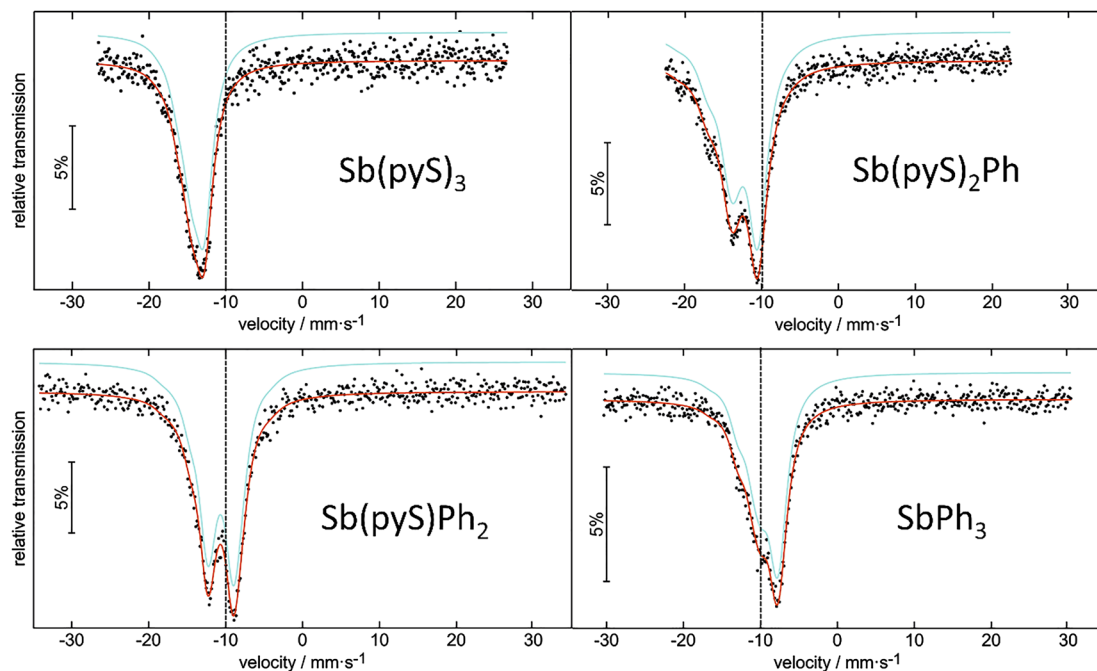


**Figure 7:** Experimental (dots) and simulated (lines)  $^{121}\text{Sb}$  Mössbauer spectra of compounds  $\text{Sb}(\text{pyS})_x\text{Ph}_{3-x}$  ( $x = 3-0$ ; 3 taken from [21]) relative to  $\text{Ba}^{121\text{m}}\text{SnO}_3$  at  $T = 5$  K. Vertical line plotted at  $-10$   $\text{mm s}^{-1}$  for comparison of the signal positions.

**Table 6:** Fitting parameters of the  $^{121}\text{Sb}$  Mössbauer spectra of compounds  $\text{Sb}(\text{pyS})_x\text{Ph}_{3-x}$  ( $x = 3-0$ ). Isomer shift  $\delta$  ( $\text{mm s}^{-1}$ ), electronic quadrupole interaction  $eQV_{zz}$  ( $\text{mm s}^{-1}$ ), experimental line width  $\Gamma$  ( $\text{mm s}^{-1}$ ) and asymmetry parameter  $\eta$ ; calculated electron density at the Sb nucleus  $\rho(0)$  ( $a_0^{-3}$ ) [55].

Compound	$\delta$	$eQV_{zz}$	$\Gamma$	$\eta$	$\rho(0)$
$\text{Sb}(\text{pyS})_3^{\text{a}}$	$-13.85(3)$	$6.1(2)$	$2.8(1)$	/	$97.06$
$\text{Sb}(\text{pyS})_2\text{Ph}$	$-12.43(2)$	$11.2(1)$	$3.13(5)$	$0.41(3)$	$92.86$
$\text{Sb}(\text{pyS})\text{Ph}_2$	$-10.74(2)$	$10.4(1)$	$2.76(5)$	$0.74(3)$	$89.28$
$\text{SbPh}_3$	$-9.28(3)$	$9.3(1)$	$2.73(6)$	/	$83.06$

<sup>a</sup>Ref. [21].

the row to lighter pnictogen central atoms (Bi, Sb, As, P), however, a slight degree of  $s/p$  hybridization was detected, and the  $\text{N} \rightarrow \text{Pn}$  interactions were found to decrease.

The set of  $\text{Sb}(\text{pyS})_x\text{Ph}_{3-x}$  ( $x = 3-0$ ) compounds was also included in this study as examples of mixed substituted  $\text{Pn}/\text{pyS}$  compounds. This stepwise substitution of  $\text{pyS}$  by  $\text{Ph}$  causes an increasing  $s/p$  hybridization of the Sb atom, *i.e.* larger  $p$  electron density of the Sb lone pair NLMO.  $^{121}\text{Sb}$  Mössbauer spectroscopy proved to be an excellent experimental probe for the calculated electronic properties of the antimony atom in these compounds, represented in the  $\delta = f[\rho(0)]$  plot ( $\delta = ^{121}\text{Sb}$  Mössbauer isomer shift,  $\rho(0) =$  calculated electron density at the Sb nucleus [55]). The set of the compounds  $\text{Pn}(\text{pyS})_3$  are valuable starting materials for the synthesis of heterobimetallic compounds

incorporating late transition metals which could feature interesting metal–metal bonding situations, a topic which we are currently investigating.

For group 13 analogues  $M^{13}(\text{pyS})_3$ , octahedral coordination of  $M^{13}$  is encountered even with  $M^{13} = \text{Al}$ . In this series ( $M^{13} = \text{In}, \text{Ga}, \text{Al}$ ), diminishing the atomic radius causes a switch from *fac* to *mer* configuration of the octahedral coordination sphere.

## 4 Experimental section

### 4.1 General considerations

All reactions have been carried out under an atmosphere of dry argon (99.999%) using standard Schlenk techniques. Solvents were dried by distillation over Na/benzophenone (THF, diethyl ether), or Na (toluene, hexane, pentane) and storage over molecular sieves 3 Å ( $\text{CHCl}_3$ , MeOH). Chemicals were purchased from ABCR ( $\text{AlEt}_3$ ,  $\text{pySH}$ ,  $\text{SbPh}_3$ ), Acros Organics ( $\text{PCl}_3$ ,  $\text{SbCl}_3$ ), AppliChem ( $\text{NEt}_3$ , further distilled from Na/benzophenone) and Sigma-Aldrich ( $\text{AsCl}_3$ ,  $\text{Bi}(\text{NO}_3)_3 \cdot 5\text{H}_2\text{O}$ ,  $n\text{-BuLi}$ ).

The melting points (not corrected) were determined on a Polytherm A microscope (Wagner & Munz, Munich, Germany). Double determinations were carried out on a crystalline sample sealed in a glass capillary.

C/H/N/S elemental analyses were performed on a vario Micro cube analyzer (Elementar, Hanau, Germany) on samples which had been dried under vacuum at room temperature. About 2 mg of the compound was placed in tin capsules and subjected to combustion in a flow of pure oxygen at  $T = 1150$  °C. The combustion gases were separated on adsorption/desorption columns and analyzed quantitatively using a thermal conductivity detector.

## 4.2 X-ray structure determinations

For single-crystal X-ray structure determination, a crystal of the appropriate size was selected under inert oil and mounted on a glass capillary, which was coated with silicone grease. Data sets were collected on an IPDS-2(T) diffractometer (STOE, Darmstadt, Germany) using graphite-monochromatized MoK $\alpha$  radiation ( $\lambda = 0.71073$  Å). Intensities were measured by  $\omega$  scans. For P(pyS)<sub>3</sub>, As(pyS)<sub>3</sub> and Al(pyS)<sub>3</sub>·0.5C<sub>7</sub>H<sub>8</sub>, numerical absorption corrections were applied by modeling the crystal surfaces based upon the intensities of symmetry-equivalent reflections (XSHAPE [56]). The structures were solved by Direct Methods (SHELXS [57]) and all non-hydrogen atoms were anisotropically refined against  $F^2$  in full-matrix least-squares cycles (SHELXL [58]). Hydrogen atoms were (isotropically) included in the refinement in geometrically idealized positions (riding model). Further details of the structure determinations of Bi(pyS)<sub>3</sub> and Al(pyS)<sub>3</sub>·0.5C<sub>7</sub>H<sub>8</sub>, including a plot of the molecular structure of the latter, are given in the Supplementary Material available online.

CCDC 1543907 [P(pyS)<sub>3</sub>], 1543895 [As(pyS)<sub>3</sub>], 2038356 [Bi(pyS)<sub>3</sub>] and 2038357 [Al(pyS)<sub>3</sub>·0.5C<sub>7</sub>H<sub>8</sub>] contain the supplementary crystallographic data for this paper. These data can be obtained free of charge from The Cambridge Crystallographic Data Centre via [www.ccdc.cam.ac.uk/data\\_request/cif](http://www.ccdc.cam.ac.uk/data_request/cif).

## 4.3 NMR spectroscopy

Solution NMR spectra were acquired on an ASCEND 400 or AVANCE 500 spectrometer (Bruker BioSpin, Rheinstetten, Germany) from samples in 5 mm glass tubes using CDCl<sub>3</sub> (99.8%, stabilized by Ag foil) as a solvent which has been dried by storage over 3 Å molecular sieves. Chemical shifts are given in ppm. The spectra were internally referenced to residual solvent signals (<sup>1</sup>H: 7.26 ppm; <sup>13</sup>C{<sup>1</sup>H} 77.16 ppm, relative to SiMe<sub>4</sub>) [59], <sup>31</sup>P{<sup>1</sup>H} was externally referenced against 85% H<sub>3</sub>PO<sub>4</sub>. The solid state <sup>13</sup>C{<sup>1</sup>H} CP/MAS NMR spectra were recorded on a AVANCE III HD 400WB spectrometer (Bruker BioSpin, Rheinstetten, Germany).

Samples were placed in 2.5 or 4 mm ZrO<sub>2</sub> rotors and an MAS frequency of 10 kHz was applied. Spectra were externally referenced to adamantane (38.5 ppm relative to SiMe<sub>4</sub>). All NMR spectra were recorded at room temperature. The positions of the pyS signals are labeled according to Hantzsch/Widman: N<sup>1</sup>-C<sup>2</sup>=S-(C<sup>3</sup>-H<sup>3</sup>)-(C<sup>4</sup>-H<sup>4</sup>)-(C<sup>5</sup>-H<sup>5</sup>)-(C<sup>6</sup>-H<sup>6</sup>) [47, 48]. In most of the <sup>1</sup>H NMR spectra, all the proton couplings within the pyS ligand could be resolved, i.e. each signal is split into three independent doublets (annotation as “d of dd”, multiplet m if coupling could not be resolved).

## 4.4 NLMO calculations

All calculations were performed using GAUSSIAN09 [60]. The hydrogen atom optimization of the atomic coordinates obtained from the X-ray diffraction analyses was performed with DFT-PBEPBE def2-TZVPP. NBO6.0 was used for the NBO/NLMO analyses [61]. DFT-B3LYP 6-311+G(d) (C, H, N, O, S, Cl, P) and SDD (As, Sb, Bi) basis sets were applied including the second order Douglas-Kroll-Hess scalar relativistic approach.

## 4.5 Mössbauer spectroscopy

For the recording of the <sup>121</sup>Sb Mössbauer spectra, the sample (ideally containing 10 mg cm<sup>-2</sup> Sb) was ground in a mortar and placed in PMMA containers of about 2 cm in diameter. The spectra were recorded at 5 K in transmission geometry. Isomer shifts are given against Ba<sup>121m</sup>SnO<sub>3</sub>, which was used as a  $\gamma$ -radiation source. The WINNORMOS for IGOR program package was used for data fitting [62].

## 4.6 Synthetic part

### 4.6.1 P(pyS)<sub>3</sub>

pySH (1.00 g, 9.00 mmol) and NEt<sub>3</sub> (1.37 g, 13.3 mmol) were dissolved in THF (15 mL) at 0 °C. Afterwards, PCl<sub>3</sub> (453 mg, 3.30 mmol) was slowly added *via* syringe, causing the formation of a white precipitate. This mixture was stirred for 2 h at this temperature. Afterwards, the HNET<sub>3</sub>Cl precipitate was filtered off and washed with THF (2 × 3 mL). The volume of the combined filtrate and washings was reduced under vacuum until crystallization of a white solid commenced (about 5 mL). This suspension was warmed slightly upon which a clear solution was obtained. The mixture was then stored at  $T = -21$  °C for 3 days, giving

colorless crystals (suitable for X-ray diffraction analysis), which were isolated by decantation, washed with diethyl ether (2 × 2 mL) and dried under vacuum. Yield: 774 mg (2.14 mmol, 71%). –  $^1\text{H}$  NMR ( $\text{CDCl}_3$ , 500.13 MHz):  $\delta = 7.05$  (d of dd,  $^3J_{\text{H-H}} = 7.3/5.0$  Hz,  $^4J_{\text{H-H}} = 1.0$  Hz, 3H, *H-5* pyS), 7.46 (m,  $^3J_{\text{H-H}} = 8.0$  Hz, 3H, *H-3* pyS), 7.54 (d of dd,  $^3J_{\text{H-H}} = 8.0/7.3$  Hz,  $^4J_{\text{H-H}} = 1.9$  Hz, 3H, *H-4* pyS), 8.33 ppm (m, 3H, *H-6* pyS). –  $^{13}\text{C}\{^1\text{H}\}$  NMR ( $\text{CDCl}_3$ , 125.77 MHz):  $\delta = 120.6$  (br, *C-5* pyS), 124.7 (br, *C-3* pyS), 136.6 (*C-4* pyS), 149.5 (br, *C-6* pyS), 157.5 ppm (br, *C-2* pyS). –  $^{31}\text{P}\{^1\text{H}\}$  NMR ( $\text{CDCl}_3$ , 202.46 MHz):  $\delta = 91.1$  ppm. – M. p. 117–121 °C. –  $\text{C}_{15}\text{H}_{12}\text{N}_3\text{PS}_3$  (361.45): calcd. C 49.84, H 3.35, N 11.63; found C 49.35, H 3.50, N 11.54.

#### 4.6.2 As(pyS)<sub>3</sub>

A solution of pySH (1.50 g, 13.5 mmol) and  $\text{NEt}_3$  (2.00 g, 19.8 mmol) in  $\text{CHCl}_3$  (20 mL) was treated with  $\text{AsCl}_3$  (816 mg, 4.50 mmol) at room temperature, causing the formation of a white solid. The solution was stirred for 2 h and then filtered and washed with  $\text{CHCl}_3$  (3 × 2 mL). This crude product was recrystallized from boiling toluene (37 mL), and crystals suitable for X-ray crystallography formed overnight by slow cooling to room temperature. The supernatant was removed by decantation, and the product was washed with toluene (2 × 2 mL) and pentane (2 × 2 mL) and dried under vacuum. Yield: 1.40 g (3.45 mmol, 77%). –  $^1\text{H}$  NMR ( $\text{CDCl}_3$ , 400.13 MHz):  $\delta = 6.98$  (d of dd,  $^3J_{\text{H-H}} = 7.4/5.0$  Hz,  $^4J_{\text{H-H}} = 1.1$  Hz, 3H, *H-5* pyS), 7.30 (m,  $^3J_{\text{H-H}} = 8.0$  Hz, 3H, *H-3* pyS), 7.49 (d of dd,  $^3J_{\text{H-H}} = 8.0/7.4$  Hz,  $^4J_{\text{H-H}} = 1.9$  Hz, 3H, *H-4* pyS), 8.20 ppm (m, 3H, *H-6* pyS). –  $^{13}\text{C}\{^1\text{H}\}$  MAS NMR (100.67 MHz,  $\nu_{\text{rot}} = 10$  kHz):  $\delta = 119.6$  (*C-5* pyS), 122.8 (*C-3* pyS), 136.3 (*C-4* pyS), 149.3 (*C-6* pyS), 161.2 ppm (*C-2* pyS). – M. p. 219–223 °C. –  $\text{C}_{15}\text{H}_{12}\text{AsN}_3\text{S}_3$  (405.40): calcd. C 44.44, H 2.98, N 10.37; found C 44.35, H 2.97, N 10.29. The product, once isolated, showed very poor solubility in common organic solvents (such as  $\text{CHCl}_3$ ,  $\text{CH}_2\text{Cl}_2$  or THF), insufficient in order to record a  $^{13}\text{C}\{^1\text{H}\}$  NMR spectrum in solution.

#### 4.6.3 Sb(pyS)<sub>3</sub>

##### 4.6.3.1 Method a

The compounds pySH (0.50 g, 4.50 mmol) and  $\text{NEt}_3$  (0.68 g, 6.72 mmol) were dissolved in THF (10 mL) and the solution was cooled to 0 °C. To this solution, solid  $\text{SbCl}_3$  (0.34 g, 1.50 mmol) was added, and the mixture was stirred and allowed to slowly attain room temperature. After 1 h, the triethylamine hydrochloride precipitate was filtered off and washed with THF (2 × 2 mL). Afterwards, gas phase diffusion of diethyl ether into the combined filtrate and

washings gave rise to the formation of colorless crystals of the product. These crystals were isolated by decantation, washed with diethyl ether (2 × 2 mL) and dried under vacuum. Yield: 0.50 g (1.10 mmol, 73%).

##### 4.6.3.2 Method b

A solution of pySH (1.00 g, 9.00 mmol) in THF (20 mL) was treated with *n*-BuLi (3.6 mL, 2.5 M in hexanes, 9.00 mmol) at –21 °C. After 15 min, solid  $\text{SbCl}_3$  (685 mg, 3.00 mmol) was added and the mixture was stirred at this temperature for 2 h after which it was allowed to attain room temperature. The solvent was removed under vacuum, and the solid residue was suspended in MeOH (10 mL) and stirred for 30 min at ambient temperature. Afterwards, the product was filtered off, washed with MeOH (3 × 2 mL) and dried under vacuum. Yield: 1.25 g (2.76 mmol, 92%). –  $^1\text{H}$  NMR ( $\text{CDCl}_3$ , 500.13 MHz):  $\delta = 6.93$  (d of dd,  $^3J_{\text{H-H}} = 7.3/5.1$  Hz,  $^4J_{\text{H-H}} = 1.1$  Hz, 3H, *H-5* pyS), 7.25 (m,  $^3J_{\text{H-H}} = 8.0$  Hz, 3H, *H-3* pyS), 7.47 (d of dd,  $^3J_{\text{H-H}} = 8.1/7.3$  Hz,  $^4J_{\text{H-H}} = 1.8$  Hz, 3H, *H-4* pyS), 8.09 ppm (d of dd,  $^3J_{\text{H-H}} = 5.1$  Hz,  $^4J_{\text{H-H}} = 1.8$  Hz,  $^5J_{\text{H-H}} = 1.0$  Hz, 3H, *H-6* pyS). –  $^{13}\text{C}\{^1\text{H}\}$  NMR ( $\text{CDCl}_3$ , 100.62 MHz):  $\delta = 118.7$  (*C-5* pyS), 124.9 (*C-3* pyS), 136.9 (*C-4* pyS), 147.1 (*C-6* pyS), 162.5 ppm (*C-2* pyS). – M. p. 203–206 °C. –  $\text{C}_{15}\text{H}_{12}\text{N}_3\text{S}_3\text{Sb}$  (452.23): calcd. C 39.84, H 2.67, N 9.29; found C 40.00, H 2.81, N 9.14.

#### 4.6.4 Bi(pyS)<sub>3</sub>

pySH (250 mg, 2.25 mmol) and  $\text{NEt}_3$  (400 mg, 3.95 mmol) were dissolved in MeOH (20 mL) and solid  $\text{Bi}(\text{NO}_3)_3 \cdot 5\text{H}_2\text{O}$  (364 mg, 0.75 mmol) was added. The resulting yellow suspension was stirred for 4 h at ambient temperature. Thereafter, the solid was filtered off, washed with MeOH (2 × 4 mL) and dried under vacuum. Yield: 360 mg (667 μmol, 89%). –  $^1\text{H}$  NMR ( $\text{CDCl}_3$ , 500.13 MHz):  $\delta = 6.95$  (d of dd,  $^3J_{\text{H-H}} = 7.3/5.2$  Hz,  $^4J_{\text{H-H}} = 1.0$  Hz, 3H, *H-5* pyS), 7.15 (d of dd,  $^3J_{\text{H-H}} = 8.1$  Hz,  $^4J_{\text{H-H}} = 1.0$  Hz,  $^5J_{\text{H-H}} = 1.0$  Hz, 3H, *H-3* pyS), 7.52 (d of dd,  $^3J_{\text{H-H}} = 8.1/7.3$  Hz,  $^4J_{\text{H-H}} = 1.8$  Hz, 3H, *H-4* pyS), 8.19 ppm (d of dd,  $^3J_{\text{H-H}} = 5.2$  Hz,  $^4J_{\text{H-H}} = 1.8$  Hz,  $^5J_{\text{H-H}} = 1.0$  Hz, 3H, *H-6* pyS). –  $^{13}\text{C}\{^1\text{H}\}$  MAS NMR (100.67 MHz,  $\nu_{\text{rot}} = 10$  kHz):  $\delta = 120.0, 127.5, 123.1, 128.5, 130.8, 138.0, 139.6, 143.2, 145.3, 147.8, 163.5, 166.1$  ppm. – M. p. 234–236 °C. –  $\text{C}_{15}\text{H}_{12}\text{BiN}_3\text{S}_3$  (539.45): calcd. C 33.40, H 2.24, N 7.79; found C 33.44, H 1.98, N 7.45. The solubility of this compound at room temperature is not sufficient to record a  $^{13}\text{C}\{^1\text{H}\}$  NMR spectrum in solution.

#### 4.6.5 Sb(pyS)<sub>2</sub>Ph and Sb(pyS)Ph<sub>2</sub>

Both compounds were prepared in a one-pot reaction starting from a mixture of  $\text{SbCl}_3$  and  $\text{SbPh}_3$  (molar ratio 1:1,

thus furnishing equal amounts of  $\text{SbCl}_2\text{Ph}$  and  $\text{SbClPh}_2$ . The final products can be easily separated by stirring of the product mixture in hot hexane ( $\text{Sb}(\text{pyS})_2\text{Ph}$  insoluble,  $\text{Sb}(\text{pyS})\text{Ph}_2$  soluble).  $\text{SbCl}_3$  (1.00 g, 4.38 mmol) and  $\text{SbPh}_3$  (1.55 g, 4.38 mmol) were heated to 150 °C for 3 h in a Schlenk tube with stirring, whereupon a brown oil formed. After cooling to room temperature, some of this oily material ( $\text{SbCl}_2\text{Ph}$  and  $\text{SbClPh}_2$ , 1.74 g, 3.00 mmol each) was slowly added to a stirred solution of pyridine-2-thiol (1.00 g, 9.00 mmol) and  $\text{NEt}_3$  (1.40 g, 13.8 mmol) in THF (40 mL) *via* syringe, upon which a white suspension formed. This suspension was stirred at 0 °C for 1 h and the mixture was filtered. The  $\text{HNEt}_3\text{Cl}$  on the filter was washed with THF (3 × 4 mL) and discarded. The solvent of the combined filtrate and washings was completely removed under vacuum, and the solid off-white residue was suspended in hexane (50 mL) and stirred at 50 °C for 30 min. The crude  $\text{Sb}(\text{pyS})_2\text{Ph}$  was then filtered off the reaction mixture, washed with hexane (2 × 5 mL) and recrystallized from boiling THF (10 mL). From the  $\text{Sb}(\text{pyS})\text{Ph}_2$ -containing filtrate, about 45 mL of hexane were distilled off, leading to the formation of colorless needles of  $\text{Sb}(\text{pyS})\text{Ph}_2$  upon cooling to room temperature. This compound was isolated by decantation, washed with cold hexane (2 × 3 mL) and dried under vacuum.

#### 4.6.5.1 $\text{Sb}(\text{pyS})_2\text{Ph}$

Yield: 690 mg (1.64 mmol, 55%). –  $^1\text{H}$  NMR (400.13 MHz,  $\text{CDCl}_3$ ):  $\delta$  = 6.90 (d of dd,  $^3J_{\text{H-H}} = 7.3/5.2$  Hz,  $^4J_{\text{H-H}} = 1.0$  Hz, 2H, *H*-5 pyS), 7.22 (m, 1H,  $\text{Ph}_{\text{para}}$ ), 7.25–7.29 (m, 4H,  $\text{Ph}_{\text{meta}}$ , *H*-3 pyS), 7.42 (d of dd,  $^3J_{\text{H-H}} = 8.3/7.2$  Hz,  $^4J_{\text{H-H}} = 1.7$  Hz, 2H, *H*-4 pyS), 8.01 (m, 2H,  $\text{Ph}_{\text{ortho}}$ ), 8.17 (m,  $^3J_{\text{H-H}} = 5.2$  Hz, 2H, *H*-6 pyS). –  $^{13}\text{C}\{^1\text{H}\}$  NMR (100.62 MHz,  $\text{CDCl}_3$ ):  $\delta$  = 118.6 (*C*-5 pyS), 124.7 (*C*-3 pyS), 128.6 ( $\text{Ph}_{\text{meta}}$ ), 128.9 ( $\text{Ph}_{\text{para}}$ ), 134.0 ( $\text{Ph}_{\text{ortho}}$ ), 136.6 (*C*-4 pyS), 147.1 (*C*-6 pyS), 147.5 ( $\text{Ph}_{\text{ipso}}$ ), 161.1 (*C*-2 pyS). – M. p. 186–190 °C. –  $\text{C}_{16}\text{H}_{13}\text{N}_2\text{S}_2\text{Sb}$  (419.18): calcd. C 45.84, H 3.13, N 6.68; found C 45.70, H 3.12, N 6.70.

#### 4.6.5.2 $\text{Sb}(\text{pyS})\text{Ph}_2$

Yield: 500 mg (1.29 mmol, 43%). –  $^1\text{H}$  NMR (500.13 MHz,  $\text{CDCl}_3$ ):  $\delta$  = 6.95 (d of dd,  $^3J_{\text{H-H}} = 7.3/5.0$  Hz,  $^4J_{\text{H-H}} = 1.0$  Hz, 1H, *H*-5 pyS), 7.32–7.38 (m, 7H,  $\text{Ph}_{\text{meta/para/H-3}}$  pyS), 7.44 (d of dd,  $^3J_{\text{H-H}} = 8.0/7.3$  Hz,  $^4J_{\text{H-H}} = 1.9$  Hz, 1H, *H*-4 pyS), 7.66 (m, 4H,  $\text{Ph}_{\text{ortho}}$ ), 8.21 (m,  $^3J_{\text{H-H}} = 5.0$  Hz, 1H, *H*-6 pyS). –  $^{13}\text{C}\{^1\text{H}\}$  NMR (125.75 MHz,  $\text{CDCl}_3$ ):  $\delta$  = 119.2 (*C*-5 pyS), 123.5 (*C*-3 pyS), 128.8 ( $\text{Ph}_{\text{meta}}$ ), 128.9 ( $\text{Ph}_{\text{para}}$ ), 135.7 ( $\text{Ph}_{\text{ortho}}$ ), 136.1 (*C*-4 pyS), 141.1 ( $\text{Ph}_{\text{ipso}}$ ), 148.8 (*C*-6 pyS), 159.6 (*C*-2 pyS). – M. p. 83–87 °C. –  $\text{C}_{17}\text{H}_{14}\text{N}_2\text{S}_2\text{Sb}$  (386.13): calcd. C 52.88, H 3.65, N 3.63; found: C 52.87, H 3.69, N 3.71. The crystals of

$\text{Sb}(\text{pyS})\text{Ph}_2$  showed a high mosaicity (broad diffraction spots) which hampered the determination of the crystal structure.

#### 4.6.6 $\text{Al}(\text{pyS})_3$

$\text{pySH}$  (0.50 g, 4.50 mmol) was dissolved in THF (30 mL) and cooled to –78 °C. At this temperature, a solution of  $\text{AlEt}_3$  in hexane (10%, 1.89 g, 1.65 mmol) was slowly added *via* syringe and stirring at –78 °C was continued for 4 h. Afterwards, the mixture was allowed to warm to room temperature and further stirred for 1.5 h. Then, the solvent of the yellowish solution was evaporated under vacuum and the solid residue was recrystallized from hot toluene (6 mL). Almost colorless (slightly yellow/beige) crystals of  $\text{Al}(\text{pyS})_3 \cdot 0.5\text{C}_7\text{H}_8$  suitable for single-crystal X-ray diffraction were isolated by decantation, washed with toluene (2 mL) and dried under vacuum. Yield: 495 mg (1.23 mmol, 82%). Upon further drying prior to elemental analysis, the crystals lost some solvent of crystallization, and the C, H, N contents found correspond to the composition  $\text{Al}(\text{pyS})_3 \cdot 0.3\text{C}_7\text{H}_8$ . –  $\text{C}_{15}\text{H}_{12}\text{AlN}_3\text{S}_3 \cdot 0.3\text{C}_7\text{H}_8$  (385.10): calcd. C 53.33, H 3.77, N 10.91; found C 52.75, H 4.04, N 10.25. –  $^{27}\text{Al}\{^1\text{H}\}$  NMR ( $\text{CDCl}_3$ , 104.26 MHz):  $\delta$  = 22.7 ppm. The  $^1\text{H}$ ,  $^{13}\text{C}\{^1\text{H}\}$  NMR data including variable-temperature experiments are listed in the Supplementary Material available online.

## 5 Supporting information

Further data on the NMR spectroscopic characterization and the crystal structure determination of  $\text{Al}(\text{pyS})_3$ , details of data collection and structure refinement of  $[\text{Bi}(\kappa^2\text{-S,N-pyS})_2(\mu\text{-S,N-pyS})]_n$ , details of the quantum chemical calculations of  $\text{Sb}(\text{pyS})\text{Ph}_2$  and  $\delta = f[\rho(0)]$  plot for the compounds  $\text{Sb}(\text{pyS})_x\text{Ph}_{3-x}$  ( $x = 3-0$ ) can be found as supplementary material in the online version (<https://doi.org/10.1515/znb-2020-0171>).

**Acknowledgments:** Dr. Erica Brendler is acknowledged for recording the solid-state  $^{13}\text{C}$  NMR spectra of  $\text{As}(\text{pyS})_3$  and  $\text{Bi}(\text{pyS})_3$ .

**Author contributions:** All the authors have accepted responsibility for the entire content of this submitted manuscript and approved submission.

**Research funding:** None declared.

**Conflict of interest statement:** The authors declare no conflicts of interest regarding this article.

## References

1. Nakatsu Y., Nakamura Y., Matsumoto K., Ooi S. *Inorg. Chim. Acta* 1992, 196, 81–88.
2. Umakoshi K., Kinoshita I., Ichimura A., Ooi S. *Inorg. Chem.* 1987, 26, 3551–3556.
3. Takashima Y., Nakayama Y., Hashiguchi M., Hosoda T., Yasuda H., Hirao T., Harada A. *Polymer* 2006, 47, 5762–5774.
4. Raper E. S. *Coord. Chem. Rev.* 1996, 153, 199–255.
5. Chadwick S., Ruhlandt-Senge K. *Chem. Eur. J.* 1998, 4, 1768–1780.
6. Pedrares A. S., Teng W., Ruhlandt-Senge K. *Chem. Eur. J.* 2003, 9, 2019–2024.
7. Chadwick S., English U., Senge M. O., Noll B. C., Ruhlandt-Senge K. *Organometallics* 1998, 17, 3077–3086.
8. Rose D. J., Chang Y. D., Chen Q., Kettler P. B., Zubieta J. *Inorg. Chem.* 1995, 34, 3973–3979.
9. Abram S., Maichle-Mössmer C., Abram U. *Polyhedron* 1997, 16, 2291–2298.
10. Chou W.-L., Chang H.-H., Yih K.-H., Lee G.-H. *J. Chin. Chem. Soc.* 2007, 54, 323–330.
11. Naktode K., Reddy T. D. N., Nayek H. P., Mallik B. S., Panda T. K. *RSC Adv.* 2015, 5, 51413–51420.
12. Dyson G., Hamilton A., Mitchell B., Owen G. R. *Dalton Trans.* 2009, 6120–6126, <https://doi.org/10.1039/b905409j>.
13. Dyson G., Zech A., Rawe B. W., Haddow M. F., Hamilton A., Owen G. R. *Organometallics* 2011, 30, 5844–5850.
14. Iannetelli A., Tizzard G., Coles S. J., Owen G. R. *Organometallics* 2018, 37, 2177–2187.
15. Zech A., Haddow M. F., Othman H., Owen G. R. *Organometallics* 2012, 31, 6753–6760.
16. Damude L. C., Dean P. A. W., Manivannan V., Srivastava R. S., Vittal J. *Can. J. Chem.* 1990, 68, 1323–1331.
17. Wächtler E., Gericke R., Kutter S., Brendler E., Wagler J. *Main Group Met. Chem.* 2013, 36, 181–191.
18. Baus J. A., Burschka C., Bertermann R., Fonseca Guerra C., Bickelhaupt F. M., Tacke R. *Inorg. Chem.* 2013, 52, 10664–10676.
19. Sousa-Pedrares A., Casanova M. I., García-Vázquez J. A., Durán M. L., Romero J., Sousa A., Silver J., Titler P. J. *Eur. J. Inorg. Chem.* 2003, 678–686, <https://doi.org/10.1002/ejic.200390094>.
20. Block E., Ofori-Okai G., Kang H., Wu J., Zubieta J. *Inorg. Chim. Acta* 1990, 190, 5–6.
21. Wächtler E., Oro L. A., Iglesias M., Gerke B., Pöttgen R., Gericke R., Wagler J. *Chem. Eur. J.* 2017, 23, 3447–3454.
22. Wächtler E., Gericke R., Block T., Pöttgen R., Wagler J. *Inorg. Chem.* 2020, 59, 15541–15552.
23. Wächtler E., Gericke R., Brendler E., Gerke B., Langer T., Pöttgen R., Zhechkov L., Heine T., Wagler J. *Dalton Trans.* 2016, 45, 14252–14264.
24. Wächtler E., Gericke R., Zhechkov L., Heine T., Langer T., Gerke B., Pöttgen R., Wagler J. *Chem. Commun.* 2014, 50, 5382–5384.
25. Daniels C. L., Knobloch M., Yox P., Adamson M. A. S., Chen Y., Dorn R. W., Wu H., Zhou G., Fan H., Rossini A. J., Vela J. *Organometallics* 2020, 39, 1092–1104.
26. Martincová J., Dostal L., Růžička A., Herres-Pawlis S., Jambor R. *Z. Anorg. Allg. Chem.* 2012, 638, 1672–1675.
27. Martincová J., Dostal L., Herres-Pawlis S., Růžička A., Jambor R. *Chem. Eur. J.* 2011, 17, 7423–7427.
28. Gericke R., Wagler J. *Inorg. Chem.* 2020, 59, 6359–6375.
29. Ehrlich L., Gericke R., Brendler E., Wagler J. *Inorganics* 2018, 6, 1–19. 119.
30. Bozopoulos A. P., Kokkou S. C., Rentzeperis P. J. *Acta Crystallogr.* 1984, C40, 944–946.
31. Block E., Ofori-Okai G., Kang H., Wu J., Zubieta J. *Inorg. Chem.* 1991, 30, 4784–4788.
32. Preut H., Huber F., Hengstmann K.-H. *Acta Crystallogr.* 1988, C44, 468–469.
33. Haikou M. N., Tsvigoulis G. M., Ioannou P. V. *Z. Anorg. Allg. Chem.* 2004, 630, 1084–1089.
34. Ioannou P. V. *Main Group Met. Chem.* 2013, 12, 125–138.
35. Buttrus N. H., Jasim Z. U., Al-Allaf T. A. K. J. *J. Appl. Sci.* 2005, 7, 92–99.
36. Haikou M. N., Ioannou P. V. *Phosphorus Sulfur* 2006, 181, 363–376.
37. Haikou M. N., Ioannou P. V. *Phosphorus Sulfur* 2006, 181, 921–929.
38. Zhang X., Lu J., Ren X., Du Y., Zheng Y., Ioannou P. V., Holmgren A. *Free Radical Biol. Med.* 2015, 89, 192–200.
39. The observation of corresponding molecular structures for the compounds  $\text{Pn}(\text{pyS})_3$  ( $\text{Pn} = \text{P}, \text{As}, \text{Sb}$ ; period 3–5 elements) contrasts with the related compounds in group 13 of the periodic table [ $\text{M}^{13}(\text{pyS})_3$ ;  $\text{M}^{13} = \text{Al}, \text{Ga}, \text{In}$ ]. Whereas for the gallium and indium compounds the *fac* isomers of the octahedral complexes are formed (see ref. [8–10]), we found the  $\text{Al}(\text{pyS})_3$  molecule to adopt the *mer* configuration in the crystal structure of its toluene solvate (see Supporting Information for details).
40. Burford N., Royan B. W., White P. S. *Acta Crystallogr.* 1990, C46, 274–276.
41. Pappalardo G. C., Chakravorty R., Irgolic K. J., Meyers E. A. *Acta Crystallogr.* 1983, C39, 1618–1620.
42. Peters M., Saak W., Pohl S. Z. *Anorg. Allg. Chem.* 1996, 622, 2119–2123.
43. Batsanov S. S. *Inorg. Mater.* 2001, 37, 871–885.
44. Ozturk I. I., Banti C. N., Hadjikakou S. K., Panagiotou N., Tasiopoulos A. J. *Inorg. Chim. Acta* 2019, 497, 119094.
45. Herzog U., Rheinwald G. J. *Organomet. Chem.* 2002, 648, 220–225.
46. Adams E. A., Kolis J. W., Pennington W. T. *Acta Crystallogr.* 1990, C46, 917–919.
47. Hantzsch A., Weber J. H. *Ber. Dtsch. Chem. Ges.* 1887, 20, 3118–3132.
48. Widman O. J. *Prakt. Chem.* 1888, 38, 185–201.
49. Moedritzer K., Maier L., Groenweghe L. C. D. J. *Chem. Eng. Data* 1962, 7, 307–310.
50. Afonin A. V., Pavlov D. V., Albanov A. I., Tarasova O. A., Nedolya N. A. *Magn. Reson. Chem.* 2013, 51, 414–423.
51. We have already reported on the spectrum of  $\text{Sb}(\text{pyS})_3$  in ref. [21]. Also, spectra of  $\text{SbPh}_3$  were already published (see ref. [52, 53]). However, we have recorded the spectrum of  $\text{SbPh}_3$  again together with the other Sb compounds using the same equipment, source and same procedure for data fitting in order to exclude systematic errors.
52. Brill T. B., Parris G. E., Long G. G., Bowen L. H. *Inorg. Chem.* 1973, 12, 1888–1891.
53. Long G. G., Stevens J. G., Tullbane R. J., Bowen L. H. *J. Am. Chem. Soc.* 1970, 92, 4230–4235.
54. Bancroft G. M., Platt R. H. *Adv. Inorg. Chem. Radiochem.* 1972, 15, 59–258.

55. Brown D. E., Johnson C. E., Grandjean F., Hermann R. P., Kauzlarich S. M., Holm A. P., Long G. *J. Inorg. Chem.* 2004, 43, 1229–1234.
56. Stoe & Cie. XSHAPE; Stoe & Cie: Darmstadt, Germany, 2002.
57. Sheldrick G. M. *Acta Crystallogr.* 2008, A64, 112–122.
58. Sheldrick G. M. *Acta Crystallogr.* 2015, C71, 3–8.
59. Fulmer G. R., Miller A. J. M., Sherden N. H., Gottlieb H. E., Nudelman A., Stoltz B. M., Bercaw J. E., Goldberg K. I. *Organometallics* 2010, 29, 2176–2179.
60. Frisch M. J., Trucks G. W., Schlegel H. B., Scuseria G. E., Robb M. A., Cheeseman J. R., Scalmani G., Barone V., Petersson G. A., Nakatsuji H., et al. GAUSSIAN 09 (revision E.01); Gaussian, Inc.: Wallingford, CT (USA), 2016.
61. Glendening E. D., Badenhoop J. K., Reed A. E., Carpenter J. E., Bohmann J. A., Morales C. M., Landis C. R., Weinhold F. NBO (version 6.0); University of Wisconsin: Madison, WI (USA), 2013.
62. Brand R. A. WINNORMOS for IGOR6 (version for IGOR 6.2 or above: 22/02/2017); Universität Duisburg: Duisburg (Germany), 2017.

---

**Supplementary Material:** The online version of this article offers supplementary material (<https://doi.org/10.1515/znb-2020-0171>).